The Astrophysical Journal, 788:154 (6pp), 2014 June 20 doi:10.1088/0004-637X/788/2/154

INTERACTION-POWERED SUPERNOVAE: RISE-TIME VERSUS PEAK-LUMINOSITY CORRELATION AND THE SHOCK-BREAKOUT VELOCITY

Eran O. Ofek[1], Iair Arcavi[1], David Tal[1], Mark Sullivan[2], Avishay Gal-Yam[1], Shrinivas R. Kulkarni[3], Peter E. Nugent[4,5], Sagi Ben-Ami[1], David Bersier[6], Yi Cao[3], S. Bradley Cenko[7], Annalisa De Cia[1], Alexei V. Filippenko[5], Claes Fransson[8], Mansi M. Kasliwal[9], Russ Laher[10], Jason Surace[10], Robert Quimby[11], and Ofer Yaron[1]

[1] Benoziyo Center for Astrophysics, Weizmann Institute of Science, 76100 Rehovot, Israel
[2] School of Physics and Astronomy, University of Southampton, Southampton SO17 1BJ, UK
[3] Cahill Center for Astronomy and Astrophysics, California Institute of Technology, Pasadena, CA 91125, USA
[4] Computational Cosmology Center, Lawrence Berkeley National Laboratory, 1 Cyclotron Road, Berkeley, CA 94720, USA
[5] Department of Astronomy, University of California, Berkeley, CA 94720-3411, USA
[6] Astrophysics Research Institute, Liverpool John Moores University, Liverpool L3 5RF, UK
[7] Astrophysics Science Division, NASA Goddard Space Flight Center, Mail Code 661, Greenbelt, MD 20771, USA
[8] Department of Astronomy, The Oskar Klein Centre, Stockholm University, AlbaNova University Centre, SE-106 91 Stockholm, Sweden
[9] Observatories of the Carnegie Institution for Science, 813 Santa Barbara St, Pasadena, CA 91101, USA
[10] Spitzer Science Center, MS 314-6, California Institute of Technology, Pasadena, CA 91125, USA
[11] Kavli IPMU (WPI), The University of Tokyo, 5-1-5 Kashiwanoha, Kashiwa-shi, Chiba 277-8583, Japan

Received 2014 February 27; accepted 2014 April 15; published 2014 June 3

ABSTRACT

Interaction of supernova (SN) ejecta with the optically thick circumstellar medium (CSM) of a progenitor star can result in a bright, long-lived shock-breakout event. Candidates for such SNe include Type IIn and superluminous SNe. If some of these SNe are powered by interaction, then there should be a specific relation between their peak luminosity, bolometric light-curve rise time, and shock-breakout velocity. Given that the shock velocity during shock breakout is not measured, we expect a correlation, with a significant spread, between the rise time and the peak luminosity of these SNe. Here, we present a sample of 15 SNe IIn for which we have good constraints on their rise time and peak luminosity from observations obtained using the Palomar Transient Factory. We report on a possible correlation between the *R*-band rise time and peak luminosity of these SNe, with a false-alarm probability of 3%. Assuming that these SNe are powered by interaction, combining these observables and theory allows us to deduce lower limits on the shock-breakout velocity. The lower limits on the shock velocity we find are consistent with what is expected for SNe (i.e., $\sim 10^4$ km s^{-1}). This supports the suggestion that the early-time light curves of SNe IIn are caused by shock breakout in a dense CSM. We note that such a correlation can arise from other physical mechanisms. Performing such a test on other classes of SNe (e.g., superluminous SNe) can be used to rule out the interaction model for a class of events.

Key words: stars: massive – stars: mass-loss – supernovae: general

Online-only material: machine-readable table

1. INTRODUCTION

A supernova (SN) exploding within an optically thick circumstellar medium (CSM) may have several unique characteristics. First, if the Thomson optical depth in the CSM is larger than c/v_s, where c is the speed of light and v_s is the shock velocity, then the shock breakout will occur in the CSM rather than near the stellar surface. This will lead to shock-breakout events that are more luminous and longer than those from normal SNe (e.g., Falk & Arnett 1977; Ofek et al. 2010; Chevalier & Irwin 2011; Balberg & Loeb 2011).

In a CSM with a slowly decreasing radial density profile (e.g., a wind profile with density $\rho \propto r^{-2}$, where r is the radial distance), the radiation-dominated shock will transform to a collisionless shock, generating hard X-ray photons and TeV neutrinos (Katz et al. 2011; Murase et al. 2011, 2014; Ofek et al. 2013a). While the collisionless shock traverses regions in which the Thomson optical depth, τ, is above a few, the hard X-ray photons can be converted to visible light (e.g., via Comptonization; Chevalier & Irwin 2012; Svirski et al. 2012). We refer to this as the optically thick interaction phase. In most cases, emission of visible light from the optically thick interaction phase will last on the order of 10 times the shock-breakout timescale (e.g., the time it takes the shock to evolve[12] from $\tau \approx 30$ to $\tau \approx 3$). Svirski et al. (2012) showed that the optically thick interaction phase is characterized by bolometric emission with a power-law or broken power-law light curve, with specific power-law indices. A recent example for such behavior was demonstrated by Ofek et al. (2014b) for SN 2010jl (PTF 10aaxf; see also Moriya et al. 2013; Fransson et al. 2013). However, in most cases the shock-breakout timescale may be less than several days, and the optically thick interaction phase will thus be short and hard to distinguish in the optical band. It is possible that later, when the interaction is moving into the optically thin region, the hard X-ray photons traveling inward toward optically thick regions (e.g., the cold dense shell; Chevalier & Fransson 1994) will be partially converted to optical photons.

Svirski et al. (2012) and Ofek et al. (2014b) showed that for SNe having light curves that are powered by interaction, there should exist a specific relation between the shock-breakout time scale, the SN luminosity, and the shock velocity at shock breakout. For various reasons the shock velocity is

[12] In a wind-profile CSM ($\rho_{CSM} = Kr^{-2}$) the optical depth is inversely proportional to the radius.

hard to measure. Ignoring the shock velocity will introduce considerable scatter into this relation. However, we still expect a correlation, with a significant spread, between the SN rise time (i.e., a proxy for the shock-breakout timescale; Ofek et al. 2010) and peak luminosity.

Type IIn SNe (e.g., Filippenko 1997) are characterized by intermediate-width emission lines which are presumably emitted by shock interaction and/or recombination in optically thin gas in the CSM due to the SN radiation field (e.g., Chevalier & Fransson 1994; Chugai 2001). Furthermore, it was suggested that hydrogen-poor superluminous SNe are powered by interaction (Quimby et al. 2011; Chevalier & Irwin 2011; see a review by Gal-Yam 2012), as well as some other rare types of SNe (e.g., Ben-Ami et al. 2014).

Here we perform a simple test of the interaction model for SNe IIn, by searching for a correlation between the rise time and peak luminosity. Indeed, we find a possible correlation between these properties. However, we stress that other models that can produce this correlation cannot yet be ruled out. We present our SN sample and observations in Section 2, and review the predictions in Section 3. The data are analyzed in Section 4, and we discuss the results in Section 5.

2. SAMPLE AND OBSERVATIONS

The Palomar Transient Factory (PTF;[13] Law et al. 2009; Rau et al. 2009) and its extension the intermediate PTF (iPTF) found over 2200 spectroscopically confirmed SNe. We selected 19 SNe IIn for which PTF/iPTF has good coverage of the light-curve rise and peak; they are listed in Table 1. Optical spectra were obtained with a variety of telescopes and instruments, including the Double Spectrograph (Oke & Gunn 1982) at the Palomar 5 m Hale telescope, the Kast spectrograph (Miller & Stone 1993) at the Lick 3 m Shane telescope, the Low Resolution Imaging Spectrometer (Oke et al. 1995) on the Keck-1 10 m telescope, and the Deep Extragalactic Imaging Multi-Object Spectrograph (Faber et al. 2003) on the Keck-2 10 m telescope. A representative spectrum of each SN is available through the WISeREP website[14] (Yaron & Gal-Yam 2012).

The PTF/iPTF data were reduced using the IPAC pipeline (Laher et al. 2014). The photometric calibration is described by Ofek et al. (2012a, 2012b). The photometry was performed by running point-spread-function fitting on subtracted images (e.g., Ofek et al. 2013c), and the photometric measurements of all SNe in our sample are listed in Table 2 and shown in Figure 1.

3. PREDICTIONS

Next we briefly review the predictions regarding the peak luminosity and rise time in the context of the interaction model. Ofek et al. (2014b) used the Chevalier (1982) self-similar hydrodynamical solution describing ejecta with a power-law velocity distribution propagating through a CSM with a power-law density distribution. Combining this with the shock-breakout properties and assuming conversion of kinetic energy into luminosity, Ofek et al. predicted a relation of the form

$$v_{\rm bo} = t_{\rm bo}^{(\alpha-1)/3}\left[2\pi\epsilon\frac{m-w}{m-3}(w-1)\frac{c}{\kappa L_0}\right]^{-1/3}. \quad (1)$$

Here $v_{\rm bo}$ is the shock-breakout velocity, $t_{\rm bo}$ is the shock-breakout timescale, ϵ is the efficiency of converting the kinetic energy to luminosity, κ is the CSM opacity, m is the power-law index of the ejecta velocity distribution, and w is the negative power-law index of the radial density profile of the CSM (i.e., $\rho = Kr^{-w}$). We note that for a wind profile CSM ($w = 2$), the mass-loading parameter is $K = \dot{M}/(4\pi v_{\rm w})$, where $\dot{M}$ is the mass-loss rate and $v_{\rm w}$ is the CSM velocity. L_0 is the luminosity extrapolated to a time of 1 s and is defined by the relations

$$L = L_0 t^{\alpha}, \quad (2)$$

and

$$\alpha = \frac{(2-w)(m-3)+3(w-3)}{m-w}. \quad (3)$$

To summarize, in interaction-powered SNe we expect a relation between $t_{\rm bo}$, $v_{\rm bo}$, and L_0 (Equation (1)). The relevant observables are the rise time, which is a proxy for the shock-breakout timescale (e.g., Ofek et al. 2010), and the peak luminosity, which is a function of L_0 and $t_{\rm bo}$. Therefore, we expect a correlation between the SN peak luminosity and its rise time. However, given the relatively large power-law index in which $v_{\rm bo}$ appears in Equation (1), relative to those of $t_{\rm bo}$ and L_0 ($v_{\rm bo}^3 \propto t_{\rm bo}^{\alpha-1}L_0$), we predict that this correlation will have a large spread (i.e., the correlation will be weak rather than tight).

4. ANALYSIS

In the context of the CSM-shock-breakout model, characterization of the SN rise time requires a model for the functional shape of the rising light curve. Although some progress has been made (e.g., Ginzburg & Balberg 2014), we still lack such a model. For simplicity, here we fit each SN rising light curve with an exponential function of the form

$$L = L_{\rm max}\{1-\exp[(t_0-t)/t_{\rm e}]\}. \quad (4)$$

Here L is the luminosity at time t, and the free parameters in the fit are the peak luminosity $L_{\rm max}$, the time when the flux is zero t_0, and the characteristic rise time $t_{\rm e}$. We note that, in our analysis, instead of using the fitted $L_{\rm max}$, we used the actual maximum observed luminosity. This was done in order to avoid the effect of a possible covariance between $t_{\rm e}$ and $L_{\rm max}$ that may arise from the fitting process. The R-band luminosity was calculated taking into account the Galactic extinction in the SN direction (Cardelli et al. 1989; Schlegel et al. 1998), the SN luminosity distance (WMAP3 cosmology; Spergel et al. 2007), and assuming that the absolute magnitude of the Sun in the $R_{\rm PTF}$ band is 4.66 mag (Ofek et al. 2012a).

We also attempted to fit a t^2 law of the form

$$L = L_{\rm max}\left(1-\left[\frac{t-t_{\rm max}}{\Delta t}\right]^2\right). \quad (5)$$

Here $t_{\rm max}$ is the maximum of the parabolic fit, and Δt is the time from zero to maximum luminosity. In this case, the characteristic rise time (i.e., the time it takes the light curve to rise by a factor of exp [1]) is given by

$$t_{\rm e} = \Delta t(1+\sqrt{1-e^{-1}}). \quad (6)$$

Both fits provide a reasonable empirical description of the rising light curves (Figure 2). For the purpose of the analysis presented here, we use the $t_{\rm e}$ obtained from the exponential fit (Equation (4)). We note that, qualitatively, the results do not change if one uses the rise time obtained from the parabolic fit.

[13] http://www.astro.caltech.edu/ptf/
[14] http://www.weizmann.ac.il/astrophysics/wiserep/

Table 1
Supernovae Sample

Name	R.A. (deg)	Decl. (deg)	z	DM (mag)	E_{B-V} (mag)	t_0 (MJD)	$t_{\max}$ (MJD)	$L_{\max}$ (erg s^{-1})	L_0 (erg s^{-1})	t_e (day)	χ^2/dof	v_{bo} (km s^{-1})	$\log_{10} K$ (g cm^{-1})
PTF10cwx	188.3189	−0.0530	0.073	37.58	0.025	55243.3	55275.3	7.2×10^{42}	4.7×10^{44}	12.7 ± 5.7	8.5/7	3300	17.0
PTF10gvf	168.4385	53.6291	0.081	37.82	0.011	55319.9	55337.5	1.0×10^{43}	5.5×10^{44}	6.6 ± 1.5	27.4/15	4600	16.7
PTF10hbf	193.1944	−6.9220	0.042	36.32	0.036	55292.1	55320.6	9.9×10^{41}	6.5×10^{43}	13.3 ± 4.4	3.9/9	1700	17.1
PTF10oug	260.1866	29.0738	0.150	39.26	0.042	55378.5	55424.4	3.3×10^{43}	2.5×10^{45}	20.9 ± 5.3	13.8/14	4600	17.2
PTF10qaf	353.9287	10.7758	0.284	40.82	0.074	55350.4	55409.4	1.7×10^{44}	1.3×10^{46}	25.6 ± 8.7	0.3/4	7400	17.3
PTF10tyd	257.3309	27.8191	0.063	37.25	0.065	55419.5	55470.5	5.3×10^{42}	4.0×10^{44}	20.4 ± 2.0	34.9/17	2500	17.2
PTF10vag	326.8270	18.1310	0.052	36.81	0.111	55445.4	55464.9	7.0×10^{42}	3.6×10^{44}	5.6 ± 2.5	16.4/4	4300	16.7
PTF10weh	261.7103	58.8521	0.138	39.06	0.032	55450.3	55526.3	5.8×10^{43}	5.8×10^{45}	54.8 ± 12.4	14.8/11	4000	17.7
PTF10yyc	69.8221	−0.3488	0.214	40.12	0.046	55476.7	55506.8	5.1×10^{43}	3.0×10^{45}	9.1 ± 3.7	26.5/14	7100	16.9
PTF10achk	46.4898	−10.5225	0.033	35.77	0.063	55534.3	55551.5	5.3×10^{42}	2.6×10^{44}	5.0 ± 1.0	54.8/10	4000	16.6
PTF11fzz	167.6945	54.1052	0.082	37.85	0.011	55723.6	55798.6	3.3×10^{43}	2.4×10^{45}	18.2 ± 1.4	121.1/19	4800	17.2
PTF12cxj	198.1612	46.4851	0.036	35.96	0.011	56029.6	56050.1	2.6×10^{42}	1.5×10^{44}	9.1 ± 1.0	93.2/51	2600	16.9
PTF12glz	238.7210	3.5354	0.079	37.76	0.131	56107.6	56155.4	3.3×10^{43}	2.7×10^{45}	26.3 ± 2.2	42.7/33	4300	17.3
PTF12ksy	62.9421	−12.4669	0.031	35.66	0.043	56232.5	56256.7	5.2×10^{42}	3.7×10^{44}	17.3 ± 6.4	136.2/12	2700	17.2
iPTF13agz	218.6338	25.1621	0.057	37.02	0.033	56377.5	56418.3	3.9×10^{42}	2.8×10^{44}	18.0 ± 2.5	76.7/58	2400	17.2
PTF09drs	226.6257	60.5943	0.045	36.49	0.017	55025.5	55066.5	5.2×10^{42}	3.7×10^{44}	17.7 ± 16.3	14.3/6	2600	17.2
PTF10cwl	189.0919	7.7939	0.085	37.93	0.022	55245.1	55261.7	9.1×10^{42}	4.5×10^{44}	5.0 ± 12.8	0.6/2	4800	16.6
PTF10tel	260.3778	48.1298	0.035	35.93	0.016	55427.8	55442.6	7.3×10^{42}	3.9×10^{44}	6.6 ± 3.5	4.3/2	4100	16.7
PTF12efc	224.1447	39.6848	0.234	40.34	0.012	56052.7	56155.5	6.8×10^{43}	7.9×10^{45}	$88.0 \pm \cdots$	18.9/19	3700	17.9

Notes. The sample of SNe IIn. DM (mag) is the distance modulus of the SN host galaxy. E_{B-V} is the Galactic extinction in the SN direction (Schlegel et al. 1998), t_0 is the MJD of the fitted zero flux, $t_{\max}$ is the MJD of the R-band light-curve peak, and $L_{\max}$ is the corresponding peak luminosity. $L_0 = L_{\max}(t/t_{bo})^{-\alpha}$, where the time is measured in seconds (e.g., Equation (2)). t_e is the exponential rise time of the early-time light curve, and v_{bo} is the lower limit on the shock velocity deduced from Equation (1) and assuming $\epsilon = 0.3$, $w = 2$, and $m = 10$; $\kappa = 0.34$ cm^2 g^{-1}. The mass-loading parameter $K = \dot{M}/(4\pi v_w)$ is calculated assuming a wind profile with $w = 2$. We assumed that the relative error in $L_{\max}$ is 20%. SNe below the horizontal line have relative errors in t_e larger than 50% and were excluded from our correlation analysis. *Information for individual objects.* PTF 09drs—Ofek et al. (2013a). PTF 10cwl (CSS100320:123622+074737)—Drake et al. (2010). PTF 10tel (SN 2010mc)—Ofek (2012), Ofek et al. (2013a), Ofek et al. (2013b). PTF 10weh—Ben-Ami et al. (2010), Ofek et al. (2014a). PTF 12efc—is a candidate Type Ia SN interacting with its CSM (Silverman et al. 2013). PTF 12cxj—Ofek et al. (2014a). PTF 12glz—Gal-Yam et al. (2012). PTF 10cwx, PTF 10gvf, PTF 10hbf, PTF 10oug, PTF 10qaf, PTF 10tyd, PTF 10vag, PTF 10yyc, PTF 10achk, PTF 11fzz, PTF 12ksy, iPTF 13agz—reported here for the first time. PTF 10cwx—a spectrum of this SN obtained during maximum light shows narrow Balmer emission lines, and possible weak He I lines, with a moderately blue continuum. Another spectrum taken about 7 weeks after maximum light still shows a blue continuum with narrow Balmer emission lines. PTF 10gvf—the first spectrum, taken about 2 weeks prior to maximum light, shows Balmer as well as He I and He II emission lines. A week later, the spectrum becomes bluer, but the He lines are not detected. Seven weeks after maximum light, the Balmer lines are still strong and become wider. PTF 10hbf—a spectrum taken about 2 weeks after maximum light shows an intermediate-width Hα line. PTF 10oug—a single spectrum of this SN taken about 27 days prior to maximum light shows a blue continuum with Balmer emission lines. PTF 10qaf—a series of spectra taken from maximum light until about three months after maximum light show Balmer emission lines. The Hβ line develops a weak P-Cygni profile about one month after maximum light. PTF 10tyd—the first spectrum was obtained about 26 days prior to peak luminosity. It exhibits a blue continuum with intermediate-width Balmer lines. A spectrum taken about one month after maximum light is very similar to the first spectrum. PTF 10vag—the first spectrum, obtained about 10 days prior to peak luminosity, shows a blue continuum with Balmer and He I emission lines. The He I lines are still visible about 20 days after maximum light. PTF 10yyc—a spectrum taken during maximum light shows a blue continuum with Balmer emission lines. PTF 10achk—two spectra taken at maximum light and 10 days later shows a blue continuum with Balmer emission lines. The first spectrum also shows He I emission lines. PTF 11fzz—the first spectrum was taken during the SN rise, about 10 days after discovery. This spectrum shows a blue continuum with Balmer and He I intermediate-width emission lines. 75 days after maximum light, the strong Balmer emission lines are still present. PTF 12ksy—the first spectrum, obtained about 20 days prior to peak luminosity, shows a blue continuum with Balmer and He I emission lines. One month later, the Hα emission line exhibits a narrow absorption at velocity of about −500 km s^{-1}, while the He I λ5876 line develops a strong P-Cygni profile. iPTF 13agz—a spectrum obtained about one month after maximum light shows a blue continuum with Balmer emission lines.

The best-fit exponential rise time and maximum luminosity for each SN are listed in Table 1.

For the 19 SNe in our sample, we estimated the errors in the rise times using the bootstrap technique (Efron 1982). For 4 out of 19 events the relative errors are larger than 50%; they appear in Table 1 below the horizontal line and are marked on the plots with gray boxes. We flagged these events as unreliable and they were not used in the correlation analysis.

Figure 2 presents the observed $L_{\max}$ versus t_e. The Spearman rank correlation of the remaining 15 SNe in our sample is 0.49. Using the bootstrap technique (Efron 1982) we find that the probability to get a correlation coefficient larger than that is 0.03. Therefore, the correlation is significant at the 2.5σ level. We note that the Spearman rank correlation is not sensitive to the distribution of variables, while the use of the bootstrap technique give us an estimate of the false-alarm probability

Table 2
Supernovae Photometry

Name	Telescope	Filter	MJD (day)	R_{PTF} (mag)	Err (mag)
PTF12ksy	PTF	R	56202.486	20.414	0.143
PTF12ksy	PTF	R	56235.251	19.175	0.098
PTF12ksy	PTF	R	56235.280	19.038	0.059
PTF12ksy	PTF	R	56237.255	18.840	0.057
PTF12ksy	PTF	R	56237.288	18.919	0.033

Notes. Photometric measurements of the SNe in the sample. This table contains measurements from the PTF/iPTF telescope as well as the Palomar 60 inch and Liverpool 2 m telescope.

(This table is available in its entirety in a machine-readable form in the online journal. A portion is shown here for guidance regarding its form and content.)

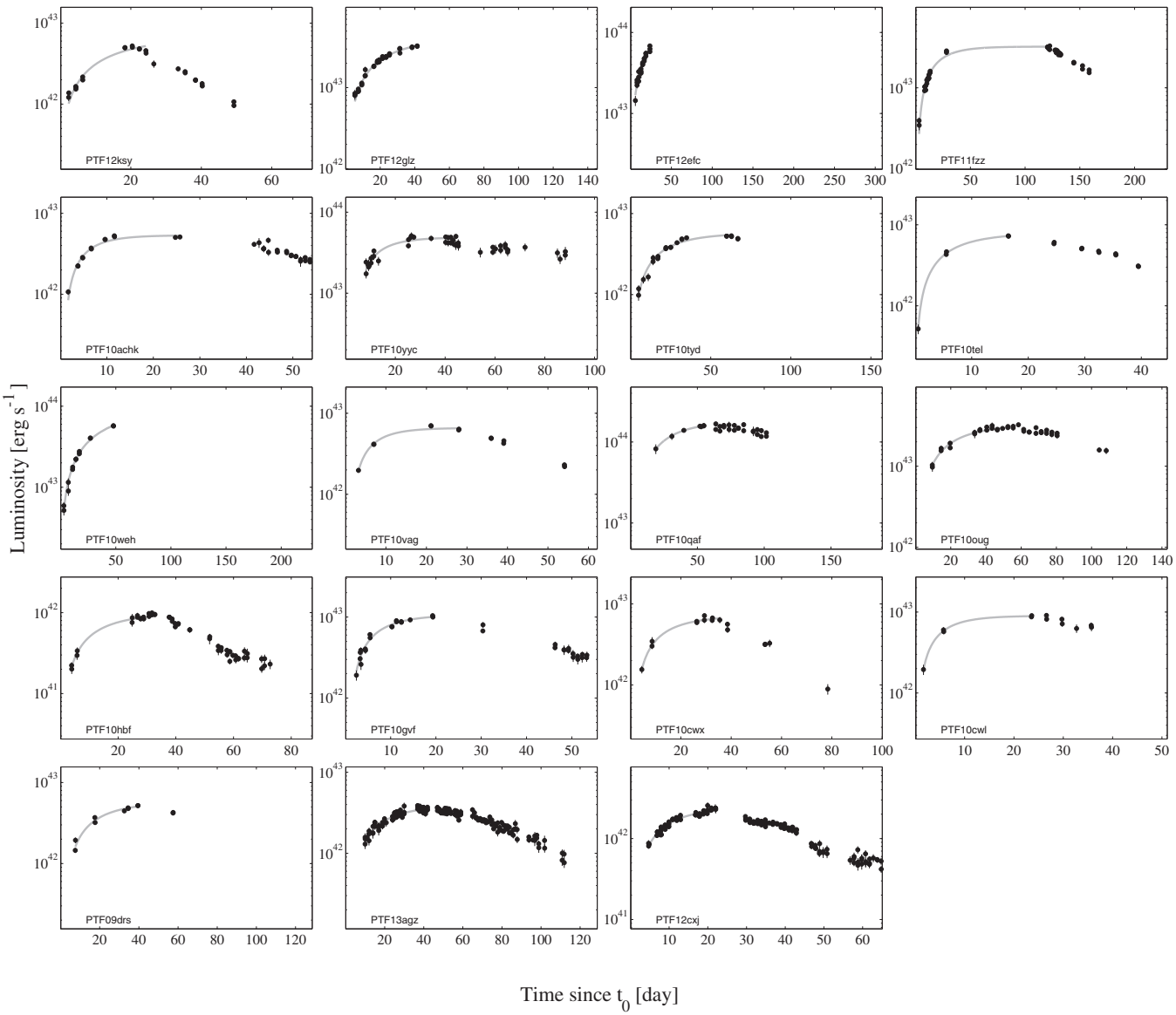

Figure 1. Light curves of the 19 SNe in our sample, for which we attempted to fit the rise time using the exponential rise function (Equation (4)). The black circles show the PTF/iPTF *R*-band measurements with their uncertainties, while the gray lines represent the best-fit exponential rise function. The SN name is marked in each subplot. The values of t_0 are listed in Table 1.

taking into account the scatter in the data, but without using the formal errors in the variables. Furthermore, we tried different statistical approaches that make quite different assumptions and obtained very similar results.

Our results may be affected by selection biases and therefore should be treated with care. A possible selection effect is that SNe with longer rise times are easier to detect even if they are faint. However, such a selection effect will introduce an anticorrelation between the rise time and peak luminosity. Another concern is if the luminosity span of the light-curve rise can affect our fitting. In order to check for this and other selection effects, we also look for correlations between the luminosity ratio of the first SN detection and its peak luminosity, and the SN rise time as well as the SN peak luminosity. We do not find any evidence for such correlations.

We conclude that there is marginal evidence for a correlation between the rise time and peak luminosity of SNe IIn, and that in this stage we cannot rule out the possibility that these SNe are powered by interaction.

Next, we use Equation (2), with the constants listed below, to calculate L_0. Figure 3 shows L_0 versus t_e. L_0 is a function of L_{max} and t_e, and therefore Figure 3 shows two nonindependent parameters. However, in Figure 2 we already showed that there is a possible correlation between an independent version of these parameters. We note that in the context of the interaction model t_e is our best estimate for t_{bo}. Most importantly, the power-law index of v_{bo} in Equation (1) is larger than that of L_0 and t_{bo}. Therefore, we expect that Figure 3 will exhibit a large scatter.

We stress that theory as well as some UV observations suggest that the bolometric rise time can be faster than the *R*-band rise time (e.g., Roming et al. 2012; Gal-Yam et al. 2014); hence, our t_e is likely only an upper limit on t_{bo}. Moreover, L_0 was estimated based on the *R*-band magnitude rather than the bolometric magnitudes. Therefore, these L_0 values should be regarded as lower limits.

Overplotted on Figure 3 are the equal shock-velocity contours, as calculated using Equation (1), assuming $w = 2$ (i.e., wind profile), $m = 12$, $\kappa = 0.34$ cm^2 r^{-1}, and $\epsilon = 0.3$. These

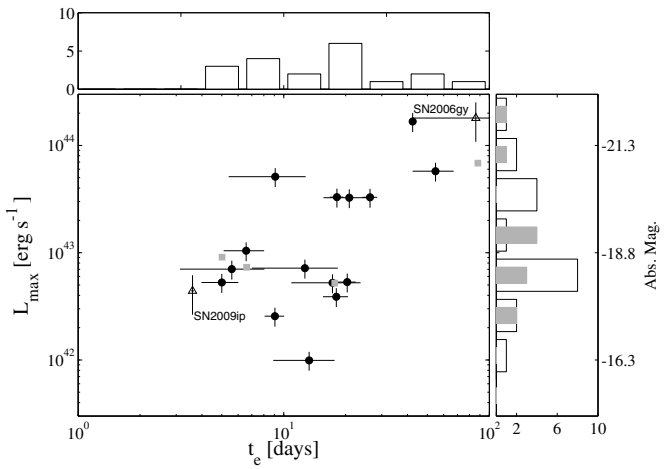

Figure 2. Peak luminosity (L_{max}) vs. exponential rise (t_e) for the SNe in our sample. The black circles are for the SNe whose relative errors on the best-fit exponential rise are smaller than 50%, while the gray squares are for all the other SNe. We did not plot the errors for the gray squares, and the corresponding SNe were not used in our correlation analysis. The white histograms on the top and right sides present the t_e and L_{max} distributions, respectively, for all 19 sources. The narrower gray bars on the right histogram show the peak absolute magnitude distribution of 11 SNe IIn discussed by Kiewe et al. (2012). Also shown (empty triangles) are the positions of some other events: SN 2006gy (Ofek et al. 2007, Smith et al. 2007) and SN 2009ip (Prieto et al. 2013, Ofek et al. 2013c, Margutti et al. 2014). The rise time for these SNe was fitted in a way similar to that for the main SNe in our sample.

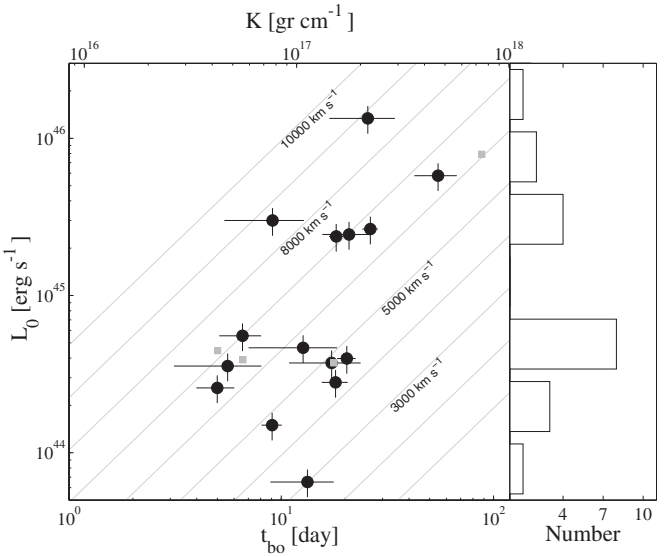

Figure 3. Shock-breakout timescale (t_{bo}) vs. L_0. The shock breakout timescale is assumed to be identical to t_e, while L_0 is calculated from Equation (2). Symbols as in Figure 2. Lines of equal shock-breakout velocity, as calculated using Equation (1), are shown as gray dashed lines. We note that, in the context of the interaction model, our measurements provide a lower limit on L_0 and t_{bo}; thus, they represent a lower limit on the breakout shock velocity. The upper abscissa gives the mass-loading parameter K assuming a wind profile (i.e., $w = 2$; see Equation (8) in Ofek et al. 2014b). The vertical histogram on the right shows the L_0 distribution for all 19 SNe in our sample.

values of m and w were also used to calculate L_0. We note that $m = 12$ (10) is expected in the case of a convective (radiative) envelope (Matzner & McKee 1999), and that the value of α is not very sensitive to the value of m (see Ofek et al. 2014b).

Furthermore, $\epsilon = 0.3$ is close to the maximum possible efficiency. Given that our measurements provide an upper limit on t_{bo} and a *lower* limit on L_0, the deduced breakout shock velocities in Figure 3 are only a lower limit on the actual shock velocity at breakout.

5. DISCUSSION

There is a growing line of evidence that SNe IIn are embedded in a large amount of CSM ejected months to years prior to their explosions (e.g., Dopita et al. 1984; Weiler et al. 1991; Chugai & Danziger 1994; Smith et al. 2008; Gal-Yam & Leonard 2009; Kiewe et al. 2012; Ofek et al. 2013c). In some cases we probably see optical outbursts associated with these mass-loss events (e.g., Foley et al. 2007; Pastorello et al. 2007; Mauerhan et al. 2013; Corsi et al. 2014; Fraser et al. 2013; Ofek et al. 2013c, 2014a). This CSM is likely to be optically thick and lead to luminous and long shock-breakout events (Ofek et al. 2010; Chevalier & Irwin 2011).

For some SNe the early-time light curve is powered by shock breakout in a dense CSM followed by conversion of the kinetic energy to optical luminosity via shock interaction in optically thick regions. In such cases, Svirski et al. (2012) and Ofek et al. (2014b) predicted a relation between the shock-breakout timescale (t_{bo}), velocity (v_{bo}), and the SN peak luminosity L_{max}.

Based on a sample of 15 SNe IIn from PTF/iPTF, we show that there is a possible correlation between their rise time and peak luminosity. Interpreting this correlation in the context of the relation predicted by Ofek et al. (2014b), the deduced lower limits on the shock velocity are consistent with the expected shock velocity from SNe (i.e., on the order of 10^4 km s^{-1}). Our findings support the suggestion made by Ofek et al. (2010) and Chevalier & Irwin (2011) that the early-time light curves of some SNe IIn are powered by shock breakout in a dense CSM. However, we note that the light curves may be contaminated by additional sources of energy (e.g., radioactivity), adding additional spread into the expected relation. Furthermore, our observations cannot yet be used to rule out other alternatives (at least not without a detailed model in hand).

In Figure 3 there is a puzzling deficiency of objects around $L_0 \approx 10^{45}$ erg s^{-1}, and maybe also some concentration of events with $L_0 \approx 4 \times 10^{44}$ erg s^{-1}. We note that comparison of the L_{max} distribution of our sample and that of 11 SNe IIn reported by Kiewe et al. (2012) suggests that this feature may be caused by small-number statistics (Figure 2). Finally, we propose that application of this test to other classes of SNe can be used to rule out the hypothesis that they are powered by interaction of their ejecta with a dense CSM.

We thank Dan Perley for obtaining some spectra. E.O.O. thanks Ehud Nakar and Orly Gnat for discussions. This paper is based on observations obtained with the Samuel Oschin Telescope as part of the Palomar Transient Factory project, a scientific collaboration between the California Institute of Technology, Columbia University, Las Cumbres Observatory, the Lawrence Berkeley National Laboratory, the National Energy Research Scientific Computing Center, the University of Oxford, and the Weizmann Institute of Science. Some of the data presented herein were obtained at the W. M. Keck Observatory, which is operated as a scientific partnership among the California Institute of Technology, the University of California, and NASA; the Observatory was made possible by the generous financial support of the W. M. Keck Foundation. We are grateful for excellent staff assistance at Palomar, Lick, and Keck Observatories. E.O.O. is incumbent of the Arye Dissentshik career development chair and is grateful to support by grants from

the Willner Family Leadership Institute Ilan Gluzman (Secaucus NJ), Israeli Ministry of Science, Israel Science Foundation, Minerva, Weizmann-UK and the I-CORE Program of the Planning and Budgeting Committee and The Israel Science Foundation. A.G-Y. acknowledge grants from the ISF, BSF, GIF, Minerva, the EU/FP7 via ERC grant (307260), and the I-CORE program of the Planning and Budgeting Committee and The Israel Science Foundation. M.M.K. acknowledges generous support from the Hubble Fellowship and Carnegie-Princeton Fellowship. A.V.F.'s SN group at UC Berkeley has received generous financial assistance from Gary and Cynthia Bengier, the Christopher R. Redlich Fund, the Richard and Rhoda Goldman Fund, the TABASGO Foundation, and NSF grant AST-1211916.

REFERENCES

Balberg, S., & Loeb, A. 2011, MNRAS, 414, 1715
Ben-Ami, S., Badenes, C., Kulkarni, S. R., et al. 2010, ATel, 2961, 1
Ben-Ami, S., Gal-Yam, A., Mazzali, P. A., et al. 2014, ApJ, 785, 37
Cardelli, J. A., Clayton, G. C., & Mathis, J. S. 1989, ApJ, 345, 245
Chevalier, R. A. 1982, ApJ, 259, 302
Chevalier, R. A., & Fransson, C. 1994, ApJ, 420, 268
Chevalier, R. A., & Irwin, C. M. 2011, ApJL, 729, L6
Chevalier, R. A., & Irwin, C. M. 2012, ApJL, 747, L17
Chugai, N. N. 2001, MNRAS, 326, 1448
Chugai, N. N., & Danziger, I. J. 1994, MNRAS, 268, 173
Corsi, A., Ofek, E. O., Gal-Yam, A., et al. 2014, ApJ, 782, 42
Dopita, M. A., Cohen, M., Schwartz, R. D., & Evans, R. 1984, ApJL, 287, L69
Drake, A. J., Djorgovski, S. G., Mahabal, A. A., et al. 2010, ATel, 2555, 1
Efron, B. 1982, The Jackknife, the Bootstrap and Other Resampling Plans (Philadelphia, PA: The Society for Industrial and Applied Mathematics)
Faber, S. M., Phillips, A. C., Kibrick, R. I., et al. 2003, Proc. SPIE, 4841, 1657
Falk, S. W., & Arnett, W. D. 1977, ApJS, 33, 515
Filippenko, A. V. 1997, ARA&A, 35, 309
Foley, R. J., Smith, N., Ganeshalingam, M., et al. 2007, ApJL, 657, L105
Fransson, C., Ergon, M., Challis, P. J., et al. 2013, arXiv:1312.6617
Fraser, M., Magee, M., Kotak, R., et al. 2013, ApJL, 779, L8
Gal-Yam, A. 2012, Sci, 337, 927
Gal-Yam, A., Arcavi, I., Ofek, E. O., et al. 2014, Natur, 509, 471
Gal-Yam, A., Ben-Ami, S., Arcavi, I., et al. 2012, ATel, 4293, 1
Gal-Yam, A., & Leonard, D. C. 2009, Natur, 458, 865
Ginzburg, S., & Balberg, S. 2014, ApJ, 780, 18
Katz, B., Sapir, N., & Waxman, E. 2011, arXiv:1106.1898
Kiewe, M., Gal-Yam, A., Arcavi, I., et al. 2012, ApJ, 744, 10
Laher, R. R., Surace, J., Grillmair, C. J., et al. 2014, arXiv:1404.1953
Law, N. M., Kulkarni, S. R., Dekany, R. G., et al. 2009, PASP, 121, 1395
Margutti, R., Milisavljevic, D., Soderberg, A. M., et al. 2014, ApJ, 780, 21
Matzner, C. D., & McKee, C. F. 1999, ApJ, 510, 379
Mauerhan, J. C., Smith, N., Filippenko, A., et al. 2013, MNRAS, 430, 1801
Miller, J. S., & Stone, R. P. S. 1993, Lick Observatory Technical Report 66 (Santa Cruz, CA: Lick Observatory)
Moriya, T. J., Maeda, K., Taddia, F., et al. 2013, MNRAS, 435, 1520
Murase, K., Thompson, T. A., Lacki, B. C., & Beacom, J. F. 2011, PhRvD, 84, 043003
Murase, K., Thompson, T. A., & Ofek, E. O. 2014, MNRAS, 440, 2528
Ofek, E. O. 2012, CBET, 3313, 1
Ofek, E. O., Cameron, P. B., Kasliwal, M. M., et al. 2007, ApJL, 659, L13
Ofek, E. O., Fox, D., Cenko, S. B., et al. 2013a, ApJ, 763, 42
Ofek, E. O., Laher, R., Law, N., et al. 2012a, PASP, 124, 62
Ofek, E. O., Laher, R., Surace, J., et al. 2012b, PASP, 124, 854
Ofek, E. O., Lin, L., Kouveliotou, C., et al. 2013b, ApJ, 768, 47
Ofek, E. O., Rabinak, I., Neill, J. D., et al. 2010, ApJ, 724, 1396
Ofek, E. O., Sullivan, M., Cenko, S. B., et al. 2013c, Natur, 494, 65
Ofek, E. O., Sullivan, M., Shaviv, N. J., et al. 2014a, arXiv:1401.5468
Ofek, E. O., Zoglauer, A., Boggs, S. E., et al. 2014b, ApJ, 781, 42
Oke, J. B., Cohen, J. G., Carr, M., et al. 1995, PASP, 107, 375
Oke, J. B., & Gunn, J. E. 1982, PASP, 94, 586
Pastorello, A., Smartt, S. J., Mattila, S., et al. 2007, Natur, 447, 829
Prieto, J. L., Brimacombe, J., Drake, A. J., & Howerton, S. 2013, ApJL, 763, L27
Quimby, R. M., Kulkarni, S. R., Kasliwal, M. M., et al. 2011, Natur, 474, 487
Rau, A., Kulkarni, S. R., Law, N. M., et al. 2009, PASP, 121, 1334
Roming, P. W. A., Pritchard, T. A., Prieto, J. L., et al. 2012, ApJ, 751, 92
Schlegel, D. J., Finkbeiner, D. P., & Davis, M. 1998, ApJ, 500, 525
Silverman, J. M., Nugent, P. E., Gal-Yam, A., et al. 2013, ApJS, 207, 3
Smith, N., Chornock, R., Li, W., et al. 2008, ApJ, 686, 467
Smith, N., Li, W., Foley, R. J., et al. 2007, ApJ, 666, 1116
Spergel, D. N., Bean, R., Doré, O., et al. 2007, ApJS, 170, 377
Svirski, G., Nakar, E., & Sari, R. 2012, ApJ, 759, 108
Weiler, K. W., Van Dyk, S. D., Discenna, J. L., Panagia, N., & Sramek, R. A. 1991, ApJ, 380, 161
Yaron, O., & Gal-Yam, A. 2012, PASP, 124, 668